J. Fluid Mech. (2001), *vol.* 435, *pp.* 305–326. Printed in the United Kingdom

On the spreading mechanism of the three-dimensional turbulent wall jet

By T. J. CRAFT AND B. E. LAUNDER

Department of Mechanical Engineering, UMIST, Manchester M60 1QD, UK

(Received 14 August 1998 and in revised form 30 November 2000)

The paper explores, using different levels of turbulence closure, the computed behaviour of the three-dimensional turbulent wall jet in order to determine the cause of the remarkably high lateral rates of spread observed in experiments. Initially, to ensure accurate numerical solution, the equations are cast into the form appropriate to a self-similar shear flow thereby reducing the problem to one of two independent variables.

Our computations confirm that the strong lateral spreading arises from the creation of streamwise vorticity, rather than from anisotropic diffusion. The predicted ratio of the normal to lateral spreading rates is, however, very sensitive to the approximation made for the pressure–strain correlation. The version that, in other flows, has led to the best agreement with experiments again comes closest in calculating the wall jet, although the computed rate of spread is still some 50% greater than in most of the measurements. Our subsequent calculations, using a forward-marching scheme show that, because of the strong coupling between axial and secondary flow, the flow takes much longer to reach its self-preserving state than in a two-dimensional wall jet. Thus, it appears very probable that none of the experimental data are fully developed.

1. Introduction

A turbulent jet of fluid, discharged from a tube into an expanse of the same fluid medium at rest, will exhibit a symmetric, linear rate of growth in all directions normal to the jet axis. If, however, the jet discharge is brought into contact with, or very close to, a plane wall whose surface is parallel with the jet axis, it is well known that a strikingly different pattern develops; for, the rate of spread of the shear flow parallel to the wall is between five and nine times as large as that normal to it (Newman *et al.* 1972; Davis & Winarto 1980; Fujisawa & Shirai 1989; Matsuda, Iida & Hayakawa 1990; Abrahamsson, Johansson & Löfdahl 1997). Although Davis & Winarto attribute the enhanced spreading to augmented turbulent diffusion parallel to the wall, the early surface streakline photographs by Newman *et al.* strongly suggested that the anisotropic growth arises from a large secondary flow causing a substantial lateral outflow parallel to the wall with a strong entrainment velocity being induced normal to the surface. This pattern has been confirmed in the recent detailed hot-wire exploration by Abrahamsson *et al.* (1997).

Progress in understanding the behaviour of this turbulent, three-dimensional wall jet has been hampered by the fact that neither numerical nor definitive experimental results for the case of laminar flow have been available. Indeed, if, as has been argued

elsewhere, Launder & Rodi (1983), vortex-line bending is the principal mechanism for creating the highly anisotropic growth, it might be surmised that laminar flows would also exhibit significantly different growth rates normal and parallel to the wall.

The purpose of the present contribution is, therefore, to remove some of the questions surrounding the turbulent wall jet. As implied above, the starting point is the laminar wall jet and thereafter, for the case of turbulent flow, different numerical solutions to the Reynolds equations are obtained based upon different strategies for approximating the Reynolds stresses. Our aim is not to undertake a fine-grained turbulence-modelling study, but rather to help clarify the underlying mechanisms by examining the broad performance of different approaches to closure. In this connection, it is helpful to begin by considering the equation for the mean streamwise vorticity, Ω_z.

$$\frac{\mathrm{D}\Omega_z}{\mathrm{D}t} = \underbrace{\Omega_x\frac{\partial W}{\partial x} + \Omega_y\frac{\partial W}{\partial y}}_{\text{mean strain bending}} + \underbrace{\Omega_z\frac{\partial W}{\partial z}}_{\substack{\text{mean strain}\\ \text{stretching/}\\ \text{compression}}}$$

$$+ \underbrace{\frac{\partial^2(\overline{v^2}-\overline{u^2})}{\partial y\,\partial x}}_{\substack{\text{turbulent normal}\\ \text{stress generation}}} + \underbrace{\frac{\partial^2\overline{uw}}{\partial x^2} - \frac{\partial^2\overline{uv}}{\partial y^2}}_{\substack{\text{turbulent shear}\\ \text{stress generation}}} + \underbrace{\nu\left(\frac{\partial^2\Omega_z}{\partial x^2} + \frac{\partial^2\Omega_z}{\partial y^2}\right)}_{\text{viscous diffusion}}. \tag{1}$$

Here, z is the primary fluid direction and the wall over which the jet develops lies in the (x, z)-plane. The vorticity components are

$$\Omega_x \equiv \left(\frac{\partial V}{\partial z} - \frac{\partial W}{\partial y}\right), \quad \Omega_y \equiv \left(\frac{\partial W}{\partial x} - \frac{\partial U}{\partial z}\right), \quad \Omega_z \equiv \left(\frac{\partial U}{\partial y} - \frac{\partial V}{\partial x}\right).$$

For the case of a laminar, three-dimensional wall jet, the first two terms in the second line of (1), expressing vorticity generation through Reynolds-stress gradients, are absent and, since the viscous terms purely diffuse vorticity, any generation of streamwise vorticity can arise only from the terms of the first row. Since the streamwise variation is, in general, much less rapid than that in the cross-sectional plane of the wall jet, it is the first two of these that are of principal importance. Their nature is most readily discerned by noting that:

$$\Omega_x\frac{\partial W}{\partial x} + \Omega_y\frac{\partial W}{\partial y} = \frac{\partial V}{\partial z}\frac{\partial W}{\partial x} - \frac{\partial U}{\partial z}\frac{\partial W}{\partial y}. \tag{2}$$

As Launder & Rodi (1983) have remarked, for the axisymmetric free jet (where $y = 0$ is a surface of symmetry) the two terms on the right-hand side of (2) exactly balance one another at all points in the flow, with the result that no secondary vorticity is created. In the wall jet, however, with $y = 0$ a non-slip surface, the second term on the right-hand side of (2) is the dominant one. For example, between the wall and the velocity maximum, W increases from zero to its maximum value over a distance y_m (figure 1) which is small compared with the flow width in the x-direction (even if, for the moment, equal growth rates in the y- and x-directions are assumed). Moreover, V may be expected to be significantly less than U since $\partial V/\partial y$ is zero at the wall, by continuity. Thus, as proposed, the sign of the vorticity generated will be determined by the second term in (2). Beyond the velocity maximum $\partial W/\partial y$ changes sign, as

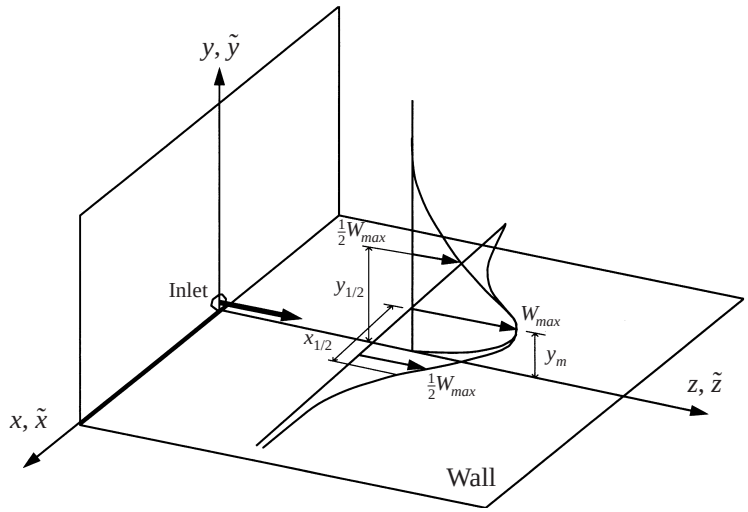

FIGURE 1. Schematic of flow considered.

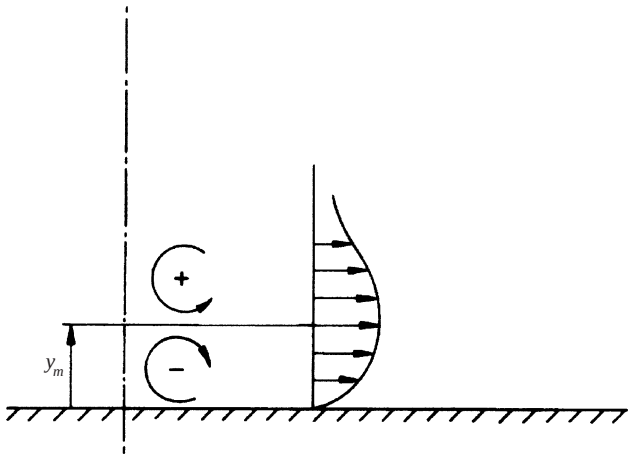

FIGURE 2. Sense of streamwise vorticity source for laminar flow.

does, in consequence, the source of streamwise vorticity. The streamwise vorticity sources are thus rather as shown in figure 2, an arrangement which evidently induces a laterally outward secondary flow.

For the case of turbulent flow, if the turbulent stresses are approximated by an eddy-viscosity representation:

$$-\overline{u_i u_j} = \nu_t \left(\frac{\partial U_i}{\partial x_j} + \frac{\partial U_j}{\partial x_i} \right) - \tfrac{2}{3}\delta_{ij} k \tag{3}$$

(k being the turbulent kinetic energy, $\frac{1}{2}\overline{u_i^2}$), then, neglecting small effects associated with streamwise velocity gradients, the turbulent stress terms on the second line of (1) may be written:

$$\frac{\partial}{\partial x}\left(\nu_t \frac{\partial \Omega_z}{\partial x} \right) + \frac{\partial}{\partial y}\left(\nu_t \frac{\partial \Omega_z}{\partial y} \right). \tag{4}$$

That is to say, the role of the turbulent stresses is reduced to that of a vorticity diffuser. The adequacy of (3) and other representations is considered later.

As implied above, the flow is a function of all three Cartesian coordinates and, as such, would not be an easy one to resolve numerically with great precision. However, the boundary conditions admit the possibility of a self-preserving flow and, indeed, some of the experiments in turbulent flow seem to suggest that a self-similar behaviour is reached within 70 jet diameters of discharge (Abrahamsson *et al.* 1997). Accordingly, the describing equations are cast in similarity coordinates, the number of independent variables thereby being reduced from three to two. The resultant equations are then solved numerically by adapting one of the available solvers to incorporate the extra terms arising from the similarity transformation. The case of laminar flow is examined first in § 2 before considering the extension to turbulent flow in § 3. Finally, it is noted that such a self-similar exploration, using a linear eddy-viscosity model, had been undertaken by Kebede (1982). That study was limited both in its scope and in the numerical accuracy that was achieved, although the qualitative performance of the model has been confirmed by more recent studies (Craft & Launder 1999).

2. Laminar flow

2.1. *Similarity form of the equations of motion*

Although the paper focuses on turbulent flow, it is helpful to consider briefly the case of laminar flow, as this flow contains some of the source terms present in the turbulent case. Moreover, it provides a simpler framework for presenting the self-similarity analysis. To simplify subsequent equations, dimensional Cartesian coordinates and the corresponding velocity components and pressure will hereinafter be shown with a tilde.

The flow considered is that arising from the discharge, from a small source at the origin, of fluid with $\tilde{z}$-directed momentum into stagnant surroundings of semi-infinite extent bounded on $\tilde{y} = 0$ by a wall. Figure 1 illustrates the resultant flow and defines certain symbols. There is a plane of symmetry along $\tilde{x} = 0$ and interest is therefore confined to the first quadrant. The external pressure is uniform (and taken as zero) and the fluid viscosity, μ, and density, ρ, are invariant. As noted, it is convenient to consider the equations of motion in dimensionless form and to this end all coordinate distances are normalised by a length L which is some characteristic width of the wall jet at any section: $x \equiv \tilde{x}/\tilde{L}$, etc. Likewise, the dimensional velocities, $\tilde{U}, \tilde{V}, \tilde{W}$ and the kinematic static pressure $\tilde{P}/\rho$ are normalized by a reference streamwise velocity W_r to form non-dimensional quantities $U \equiv \tilde{U}/W_r$, $P \equiv \tilde{P}/\rho W_r^2$ etc. The specific choice of L and W_r will be discussed later. Solutions are sought only to the self-similar flow in which the dimensionless velocity distributions are independent of $\tilde{z}$, i.e. $U = U(x, y)$; $V = V(x, y)$; $W = W(x, y)$. Following the indicated manipulations, the equations of motion describing this situation may be written:

x-momentum:

$$\frac{\partial}{\partial x}UU + \frac{\partial}{\partial y}VU = -\frac{\partial P}{\partial x} + \beta\left(x\frac{\partial WU}{\partial x} + y\frac{\partial WU}{\partial y}\right) - 2\alpha WU + \frac{\partial}{\partial x}\left(R^{-1}\frac{\partial U}{\partial x}\right) + \frac{\partial}{\partial y}\left(R^{-1}\frac{\partial U}{\partial y}\right), \tag{5}$$

y-momentum:

$$\frac{\partial}{\partial x}UV + \frac{\partial}{\partial y}VV = -\frac{\partial P}{\partial y} + \beta\left(x\frac{\partial WV}{\partial x} + y\frac{\partial WV}{\partial y}\right) - 2\alpha WV + \frac{\partial}{\partial x}\left(R^{-1}\frac{\partial V}{\partial x}\right) + \frac{\partial}{\partial y}\left(R^{-1}\frac{\partial V}{\partial y}\right), \tag{6}$$

z-momentum:

$$\frac{\partial}{\partial x}UW + \frac{\partial}{\partial y}VW = -2\alpha P + \beta\left(x\frac{\partial P}{\partial x} + y\frac{\partial P}{\partial y}\right) + \beta\left(x\frac{\partial W^2}{\partial x} + y\frac{\partial W^2}{\partial y}\right) - 2\alpha W^2 + \frac{\partial}{\partial x}\left(R^{-1}\frac{\partial W}{\partial x}\right) + \frac{\partial}{\partial y}\left(R^{-1}\frac{\partial W}{\partial y}\right), \tag{7}$$

continuity:

$$\frac{\partial U}{\partial x} + \frac{\partial V}{\partial y} = \beta\left(x\frac{\partial W}{\partial x} + y\frac{\partial W}{\partial y}\right) - \alpha W. \tag{8}$$

In the above, R denotes the reference Reynolds number $W_r L/\nu$ which is to be regarded as an independent parameter of the solution, while α and β stand for the velocity-decay and jet-spread parameters $(L/W_r)(\mathrm{d}W_r/\mathrm{d}z)$ and $\mathrm{d}L/\mathrm{d}\tilde{z}$. (In laminar flow, since ν is invariant, R is uniform over the (x, y)-plane and could be removed through the differential operators. The slightly more cumbersome form retained here illustrates how equations (5)–(7) (with an appropriate redefinition of R) serve also for the case of turbulent flow when the turbulent stresses are approximated by a turbulent viscosity model.) The boundary conditions on the velocity field are:

$$\text{At } y = 0\text{: } U = V = W = 0; \quad x = 0\text{: } U = 0; \quad \partial V/\partial x = \partial W/\partial x = 0;$$

$$y \to \infty\text{: } U = V = W = 0; \quad x \to \infty\text{: } U = V = W = 0.$$

For numerical solution, a further rearrangement of the mass and momentum sources on the right-hand sides of these equations is helpful. With the definitions $U^* \equiv U - \beta W x$; $V^* \equiv V - \beta W y$ the momentum and continuity equations may be written:

$$\frac{\partial}{\partial x}U^*U + \frac{\partial}{\partial y}V^*U = -2(\beta+\alpha)WU - \frac{\partial P}{\partial x} + \frac{\partial}{\partial x}\left(R^{-1}\frac{\partial U}{\partial x}\right) + \frac{\partial}{\partial y}\left(R^{-1}\frac{\partial U}{\partial y}\right), \tag{9}$$

$$\frac{\partial}{\partial x}U^*V + \frac{\partial}{\partial y}V^*V = -2(\beta+\alpha)WV - \frac{\partial P}{\partial y} + \frac{\partial}{\partial x}\left(R^{-1}\frac{\partial V}{\partial x}\right) + \frac{\partial}{\partial y}\left(R^{-1}\frac{\partial V}{\partial y}\right), \tag{10}$$

$$\frac{\partial}{\partial x}U^*W + \frac{\partial}{\partial y}V^*W = -2(\beta+\alpha)WW - 2(\beta+\alpha)P + \beta\left(\frac{\partial Px}{\partial x} + \frac{\partial Py}{\partial y}\right) + \frac{\partial}{\partial x}\left(R^{-1}\frac{\partial W}{\partial x}\right) + \frac{\partial}{\partial y}\left(R^{-1}\frac{\partial W}{\partial y}\right), \tag{11}$$

$$\frac{\partial}{\partial x}U^* + \frac{\partial}{\partial y}V^* = -(2\beta+\alpha)W. \tag{12}$$

In this form the effective convecting velocities in the x- and y-directions are seen to be U^* and V^*.

It remains to assign the parameters α and β. Let us first consider the simpler case of an axisymmetric free jet. This flow is equally described by equations (1)–(4) (though, of course, not as compactly as if cylindrical polar coordinates were employed). Within the thin-shear flow approximation the streamwise momentum of the free jet is conserved and so:

$$\frac{\mathrm{d}}{\mathrm{d}\tilde{z}}\left(\int_0^\infty\int_0^\infty \tilde{W}^2\,\mathrm{d}\tilde{x}\,\mathrm{d}\tilde{y}\right)=0,$$

which implies:

$$\frac{\mathrm{d}}{\mathrm{d}\tilde{z}}(W_r^2L^2)=0$$

or

$$\alpha+\beta=0. \tag{13}$$

We may arbitrarily assign β as unity, a choice that essentially fixes the scale of L, and thus α is equal to -1.

For the case of a plane wall jet, we may still apply condition (13) to a fair degree of approximation (Glauert 1956). Momentum loss through wall friction is rather more significant for the three-dimensional wall jet considered here, however (Launder & Rodi 1981). Moreover, in the case of turbulent motion considered in §3, the experimentally observed flow spreads sufficiently rapidly in the lateral direction to raise at least the question of whether it is adequate to neglect the variation of static pressure across the wall jet. This variation is proportional to W_r^2 which in turn varies with $\tilde{z}$, and so a net contribution is made to the integral force-momentum balance:

$$\frac{\mathrm{d}}{\mathrm{d}\tilde{z}}[W_r^2L^2(A+B)]=-\int_0^\infty L\frac{\tau_w}{\rho}\,\mathrm{d}x, \tag{14}$$

where τ_w is the $\tilde{z}$-component of the shear stress at a point on the wall and A and B denote the kinematic momentum and pressure integrals:

$$A\equiv\int_0^\infty\int_0^\infty W^2\,\mathrm{d}x\,\mathrm{d}y,\quad B\equiv\int_0^\infty\int_0^\infty P\,\mathrm{d}x\,\mathrm{d}y.$$

Note that A and B are independent of $\tilde{z}$, so that on expanding the differential and introducing the definitions of α and β given above we find

$$\alpha+\beta=-\sigma, \tag{15}$$

where

$$\sigma\equiv\frac{1}{2(A+B)}\int_0^\infty\frac{\tau_w}{\rho W_r^2}\,\mathrm{d}x. \tag{16}$$

Again, we take $\beta=1$ and hence $\alpha=-(1+\sigma)$.

The quantity σ is not, of course, freely assignable and must be repeatedly computed during the course of what is necessarily an iterative solution of equations (5)–(8), a topic which is considered next.

2.2. *Numerical solution procedure*

The equations of motion in similarity form provide a set of coupled, nonlinear, elliptic equations describing the dynamic field in terms of the independent variables x and y. The general-purpose elliptic solver STREAM (Lien & Leschziner 1993) has provided a convenient framework for the numerical solution of equations (9)–(12). Although these equations contain numerous 'source' and 'sink' terms which are absent from

the two-dimensional Navier–Stokes equations, the computer program is organized to allow the inclusion of such sources without adaptation to its structure. The basic scheme has been widely applied so that here it perhaps suffices to note that this finite-volume procedure based on a collocated mesh provides an ADI line solution of the discretized Navier–Stokes equations in primitive-variable form. It adopts the SIMPLE algorithm of Patankar & Spalding (1972) (as adapted for a collocated grid by Rhie & Chow 1983) to introduce perturbations to the pressure field to reduce successively the local failure of the velocity field to comply with continuity, eventually to insignificant levels.

In the present adaptation of the scheme the principal modifications to the solving procedure are:

(i) The use of U^* and V^* as the convecting velocities in the three momentum equations and the continuity equation (in place of U and V).

(ii) The introduction of a sink $-(1-\sigma)W$ in the continuity equation (with consequent repercussions on the pressure–perturbation calculation).

(iii) The incorporation, in each of the momentum equation subroutines, of terms corresponding to the extra source term $2\sigma W\phi$ (where ϕ denotes U, V or W) and, in the streamwise momentum equation, to the additional terms containing pressure.

(iv) Following each cycle of iteration, the evaluation of σ and the restoration of the initially prescribed jet momentum. The latter is achieved by multiplying each velocity component at every node by the square root of the ratio of the prescribed momentum flux to the actual value; the pressure (which is zero in the free stream) is correspondingly multiplied by the ratio itself.

The numerical solutions are obtained within the rectangular domain $0 < x < X$; $0 < y < Y$ where the outer limits X and Y are chosen, by trial and error, so that computed rates of spread are insensitive to the boundary location. A mildly expanding mesh from the origin was adopted with a geometric expansion ratio of up to 4% in the y-direction and 1% in the x-direction. Up to 60 nodes in the x-direction and 60 in the y-direction were employed, which was sufficient to achieve grid-independence when convective transport was approximated by the MUSCL scheme of Van Leer (1979).

Along $x = 0$ and $y = 0$, boundary conditions as stated in § 2.1 were applied. Along $x = X$ and $y = Y$, although W was set to zero, some variation was necessary from the conditions strictly applicable to U and V at infinity; for, if these had been set to zero, entrainment processes would not have been adequately represented. Instead, the velocity component parallel to the outer surface (i.e. V along $x = X$ and U along $y = Y$) was set to zero while the velocity normal to the surface was obtained by requiring a mass balance for each of the cells lying along these outer boundaries (no pressure–perturbation equation is solved for these cells, so a uniform pressure is applied at the outer edge of the domain). The efficacy of this scheme was established by applying it first to the free jet, as discussed in § 2.3.

2.3. *Computed behaviour for laminar flow*

Preliminary calculations were made of the free axisymmetric jet by replacing the wall at $y = 0$ by a plane of symmetry. The aim was to compare the results with the analytic solution of Schlichting (1933) thereby to assess the general accuracy of the scheme and the suitability of the outer boundary conditions of U and V. A 40×40 grid was employed. Results were obtained for values of the jet Reynolds number $W_{max}\, r_{1/2}/\nu$ ranging from 13 to 203; typical results are compared with Schlichting's solution in

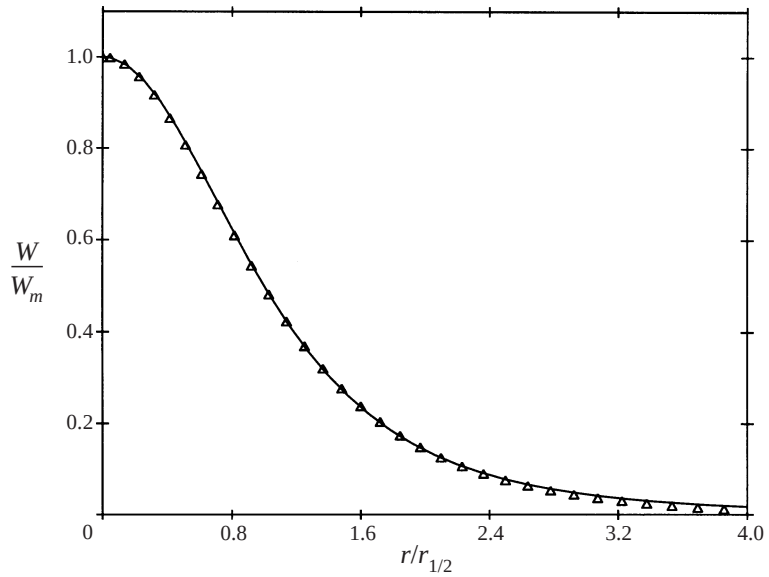

FIGURE 3. Validation of approach for axisymmetric free jet. ▽, present calculations; ———, Schlichting (1933).

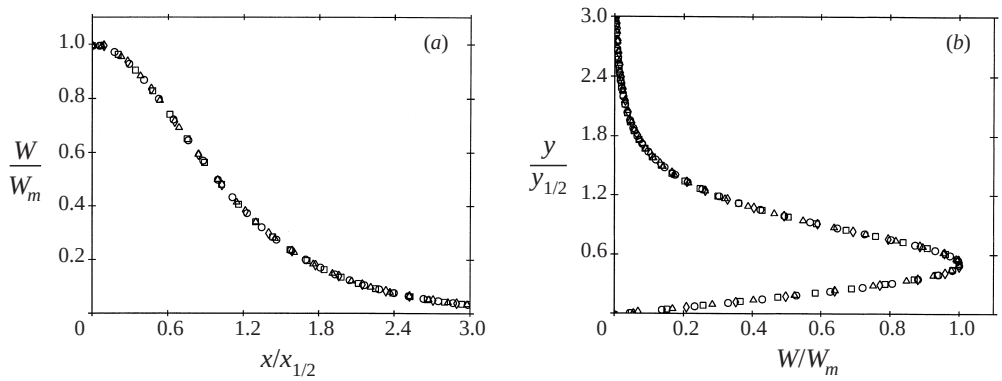

FIGURE 4. Mean velocity profiles for laminar wall-jet. ○, $R_{1/2} = 38$; □, $R_{1/2} = 77$; △, $R_{1/2} = 155$; ◇, $R_{1/2} = 308$.

figure 3. It can be seen that the numerical result is in very close agreement with the analytical solution. The result shows that the convenient but not rigorously exact outer boundary conditions adopted in this study produce negligible contamination of the flow field.

The wall-jet results were obtained by replacing the plane of symmetry by a no-slip boundary along $y = 0$. Fifty per cent more nodes were added in the direction normal to the wall concentrated, as noted in § 2.2, predominantly in the near-wall region.

The primary mean velocity distributions on the symmetry plane and along the constant-y line passing through the point of maximum velocity are shown in figure 4 for four Reynolds numbers. There is no detectable variation of the profile shape with R. An x–y mapping of the streamwise velocity contours is shown in figure 5 with the secondary velocities in the (x, y)-plane superimposed. The isovels are nearly elliptic in shape with a centre that moves away from the wall as W/W_m decreases.

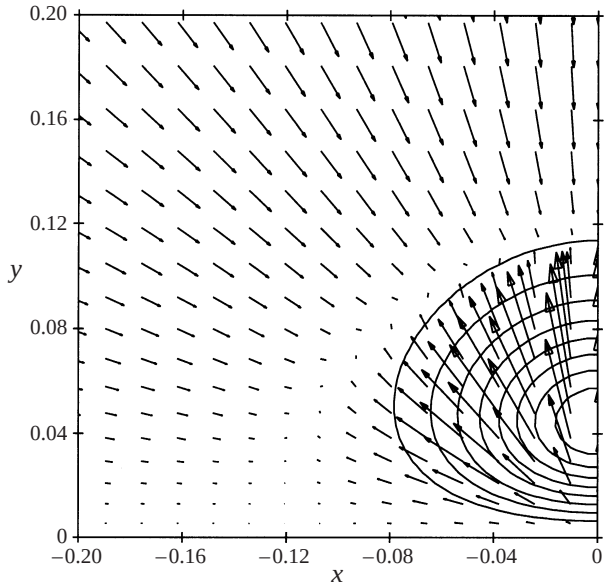

FIGURE 5. Axial velocity contours and secondary flow vectors laminar wall jet, $R_{1/2} = 155$.

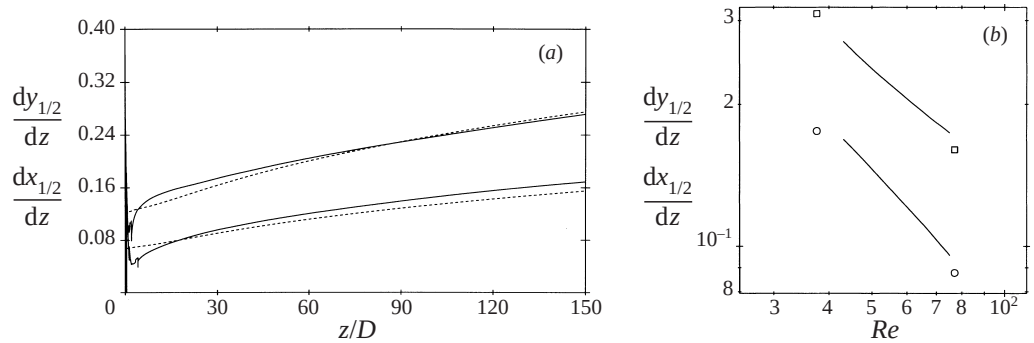

FIGURE 6. Rate of variation of spreading rates. (*a*) Downstream development. ——, parabolic, 3D marching solution; – – –, self-similar spreading rate at same Reynolds number. (*b*) Dependence on Reynolds number. Symbols: self-similar solution; ——, 3D marching solution (note the development is from right to left as Reynolds number decreases downstream).

No substantial streamwise vorticity is created and consequently the magnitude of $x_{1/2}/y_{1/2}$ is appreciably less than unity. Thus, the mechanism of vortex-line bending illustrated in figure 2 seems to be insignificant in the case of the laminar wall jet: the growth principally arises from viscous diffusion.

Before leaving the case of laminar flow, we should consider the appropriateness of an idealization implicit in the analysis, namely that each solution is strictly for a constant Reynolds number. Yet, in practice, as a wall jet develops downstream, unlike the free jet noted above, the local Reynolds number will continuously decrease owing to the loss of momentum by wall friction. To explore further the significance of this fact, the laminar wall jet was recomputed using a streamwise-marching three-dimensional 'parabolic' solver. Thus, no presumptions of self-similarity were made. Several features emerge from the results shown in figure 6. First, over the distance

considered, there is an appreciable change in $\dot{x}_{1/2}$ and $\dot{y}_{1/2}$ with distance downstream – that is, apparently, an equilibrium condition is never reached. However, locally, it can be seen that the developing flow behaviour accords very closely with the growth rate obtained from the self-similar solution at the same Reynolds number. Thus, while the Reynolds number changes throughout its development, the laminar wall jet essentially passes through a succession of self-similar states. This is further brought out in figure 6(*b*) where the abscissa is the Reynolds number, and the logarithmic scales enable us to note that the growth rates vary very nearly as R^{-1}. (This result could have been directly inferred by introducing new variables $\bar{x} \equiv xR$ and $\bar{y} \equiv yR$ into equations (9)–(12) which render the equations independent of Reynolds number save for secondary pressure-gradient terms in the streamwise momentum equation which are neglected in the usual parabolic approximation.)

3. Turbulent flow

3.1. *Preliminary observations*

The spreading pattern reported above for laminar flow is very different from that observed in turbulent flow. The differences must be attributable to the Reynolds stresses as these terms are the only ones that make the Reynolds equations different from the Navier–Stokes equations. However, there are several conceivable mechanisms by which the turbulent stress field might produce the strongly anisotropic growth pattern observed in experiments and, while an exhaustive exploration lies beyond the scope of the present contribution, some discrimination between the various possibilities can be made. The following potential mechanisms are noted:

(i) The Reynolds shear stresses opposing the primary flow produce a differently shaped (primary) velocity profile than in laminar flow with the velocity maximum lying much closer to the wall. These changes will alter the relative magnitude of the mean-strain terms generating streamwise vorticity.

(ii) The anisotropy of the Reynolds stress field can provide a direct source of streamwise vorticity (Brundrett & Baines 1964). In non-axisymmetric turbulent flows through long, straight ducts, this is the sole mechanism that drives the weak but influential secondary velocity field found in such situations.

(iii) Anisotropic turbulent diffusion associated with the mean square velocity-fluctuations parallel to the wall being appreciably larger than in the normal direction would tend to raise lateral diffusion rates relative to those normal to the wall. This effect can be important in heat diffusion in an axisymmetric flow through a circular pipe where a circumferential temperature variation exists (Black & Sparrow 1970; Chieng & Launder 1979).

(iv) High static pressure on the surface centreline has also been suggested as a means of provoking rapid lateral spreading – by a mechanism analogous to that by which a jet of warm water discharged at the free surface of a cold pool exhibits a rapid lateral spread, thereby reducing the potential energy of the system comprising the jet and the pool (see, for example, McGuirk & Rodi 1978).

If mechanism (i) were the principal contributor, at least the main effects should be reproduced by one of the popular turbulent viscosity models. However, earlier studies by Kebede (1982), employing a linear k–ε model, failed to reproduce the large lateral spreading rate. Although recent work by Craft & Launder (1999) concluded the Kebede's calculations were not entirely grid-independent, they did confirm his findings that eddy-viscosity models grossly underpredicted the lateral spreading

rate, with computations predicting a lateral to wall-normal spreading rate ratio of only 0.9.

For either of mechanisms (ii) and (iii), a turbulence closure based on the Reynolds-stress equations must be adopted, whether in full transport form or some simpler derivative. To distinguish the relative importance of these two processes (i.e. vorticity source versus anisotropic diffusion) it suffices to make a calculation in which the turbulent stresses in the streamwise momentum equation are represented by the stress-transport model while those in the U- and V-momentum equations are computed by a turbulent viscosity formula, thereby removing the contribution of turbulent stresses to the creation of streamwise vorticity. Moreover, within the framework of a stress-transport closure, different hypotheses can be explored for the 'redistribution' of the Reynolds stress caused by pressure fluctuations. Finally, the importance of integrating the equations of motion through the thin viscous sublayer immediately adjacent to the wall merits examination, for the alternative practice of applying the 'universal' semi-logarithmic velocity law outside the viscous layer considerably reduces computational effort.

In the following section, the above matters, as well as the recurrent question of numerical accuracy will be examined.

3.2. *Application of second-moment modelling*

Second-moment closure, based on transport equations for the Reynolds stresses, provides a level of modelling at which one might hope to mimic to satisfactory engineering accuracy (of, say, $\pm 15\%$) the development of the three-dimensional wall jet. In Cartesian tensor notation the equation describing the transport of the Reynolds stress $\overline{u_i u_j}$ may be written:

$$\begin{aligned}
\frac{\mathrm{D}\,\overline{u_i u_j}}{\mathrm{D}t} = & -\left\{ \overline{u_i u_k}\,\frac{\partial U_j}{\partial x_k} + \overline{u_j u_k}\,\frac{\partial U_i}{\partial x_k} \right\} && P_{ij} \\
& -2\nu\,\overline{\frac{\partial u_i}{\partial x_k}\,\frac{\partial u_j}{\partial x_k}} && \varepsilon_{ij} \\
& +\overline{\frac{p}{\rho}\left(\frac{\partial u_i}{\partial x_j} + \frac{\partial u_j}{\partial x_i}\right)} && \phi_{ij} \\
& -\frac{\partial}{\partial x_k}\left(\overline{u_i u_j u_k} + \frac{\overline{p u_i}}{\rho}\,\delta_{jk} + \frac{\overline{p u_j}}{\rho}\,\delta_{ik} \right) && d_{ij} \\
& +\frac{\partial}{\partial x_k}\left(\nu \partial\,\frac{\overline{u_i u_j}}{\partial x_k} \right) && d^{\nu}_{ij}
\end{aligned} \tag{17}$$

The column of symbols on the right-hand side opposite each term of the equation indicates the shorthand notation to be used for each of the processes.

While the shear production (P_{ij}) and molecular diffusion (d^{ν}_{ij}) can be handled without approximation, models must be provided for each of the other three agencies. For the fully turbulent region, the usual assumptions of local isotropy (for the dissipation, ε_{ij}) and the generalized gradient diffusion hypothesis (d_{ij}) are adopted:

$$\varepsilon_{ij} = \tfrac{2}{3}\delta_{ij}\varepsilon, \tag{18}$$

$$d_{ij} \equiv \frac{\partial}{\partial x_k}\left(c_s \overline{u_k u_l}\,\frac{k}{\varepsilon}\,\frac{\partial}{\partial x_l}\,\overline{u_i u_j} \right). \tag{19}$$

The latter, due to Daly & Harlow (1970), is far short of the best-known model for stress diffusion, but it is retained on the grounds that it creates few, if any, numerical problems while in most wall flows the term, in any event, is of only marginal significance.

For the three-dimensional wall jet, the most sensitive term (it will be seen) is the pressure-strain correlation, ϕ_{ij}. The behaviour resulting from three models is considered. The most commonly used model for this process is the two-part isotropization model:

$$\phi_{ij} = -c_1 \frac{\varepsilon}{k}(\overline{u_i u_j} - \tfrac{2}{3}\delta_{ij}k) - c_2(P_{ij} - \tfrac{1}{3}\delta_{ij}P_{kk}), \tag{20}$$

a level that will be termed Model 1. However, it is widely known that, in flows near walls, a 'wall-echo' term must be added to (20) in order (principally) to redistribute some of the fluctuating turbulent energy normal to the wall to directions parallel to the surface. There are several proposals in the literature dating back over twenty years. However, we adopt the relatively recent proposal due to Craft & Launder (1992) because it was devised to cope both with parallel shear flows and with impinging flows (the three-dimensional turbulent wall jet being a shear flow that is a cross between the two). Thus:

$$\phi_{ij}^{w} = \left\{ -0.08 \frac{\partial U_l}{\partial x_m} \overline{u_l u_m}(\delta_{ij} - 3n_i n_j) + 0.4k \frac{\partial U_l}{\partial x_m} n_l n_m (n_i n_j - \tfrac{1}{3}\delta_{ij}) \right.$$
$$\left. -0.1(\overline{u_l u_m} - \tfrac{2}{3}\delta_{lm}k)\left(\frac{\partial U_k}{\partial x_m} n_l n_k \delta_{ij} - \frac{3}{2}\frac{\partial U_i}{\partial x_m} n_l n_j - \frac{3}{2}\frac{\partial U_j}{\partial x_m} n_l n_i \right) \right\} \frac{l}{2.5y}, \tag{21}$$

where $l \equiv k^{3/2}/\varepsilon$, n_j is the unit vector normal to the wall and y (as here) denotes the distance of a point from the wall. Model 2 is thus (20) plus the correction given by (21).

In practice, wall corrections of the type adopted in Model 2 are of no use in complex topographies, for the rigid surfaces are not plane and of, effectively, infinite extent. Newer approaches have thus been concerned with developing models of wider validity. Durbin and co-workers (Durbin 1993; Wizman *et al.* 1996) have proposed an 'elliptic relaxation' in which the algebraic wall correction, (21), is replaced by an integro-differential equation. An alternative approach, followed by the authors and others, has been to devise a more widely applicable form of ϕ_{ij} so that no wall-correction is necessary. The strategy is to construct a model that satisfies the two-component limit (TCL) to which turbulence reduces at a wall (Lumley 1978; Shih & Lumley 1985; Fu *et al.* 1987; Craft, Launder & Ince 1996); equation (21) is then not employed. This latter approach was originally devised by reference to free shear flows (Fu 1988), but has recently been applied to quite complicated flows in ducts and pipe bends returning distinctly better agreement with experiment than that resulting from employing (20) and (21) (Launder & Li 1994; Iacovides, Launder & Li 1996). In the present work, the form used by these workers is adopted, Model 3. All the above schemes have adopted local-equilibrium wall functions to bridge the viscous sublayer, though summary results are also included for the later form of Model 3 by Craft (1997) which enables computations to be extended through the viscous sublayer up to the wall. Even in tensor notation (see the Appendix) the algebraic form of Model 3 is fairly cumbersome but, because it cannot generate unrealizable values of the Reynolds stresses, actual computation times are usually no longer than for the simple return-to-isotropy form.

In all three models, closure is completed by solving, in parallel with the stress

Source	$\frac{dy_{1/2}}{dz}$	$\frac{dx_{1/2}}{dz}$	$\frac{\dot{x}_{1/2}}{\dot{y}_{1/2}}$	$\frac{U_m}{W_m}$
Experiment (Abrahamsson *et al.* 1997)	0.065	0.320	4.94	0.20
Model 1. Isotropization model without wall reflection	0.081	0.079	0.97	0.017
Model 2. Isotropization model including equation (20) for wall reflection	0.053	0.814	15.3	0.44
Model 3. TCL closure	0.064	0.53	8.26	0.28
TCL closure due to Craft (1997) (integration to wall)	0.060	0.51	8.54	0.27

TABLE 1. Comparison of spreading in the three-dimensional turbulent wall jet using stress-transport closures.

transport equations, an equation for ε. The form used with Models 1 and 2 is:

$$\frac{D\varepsilon}{Dt} = c_{\varepsilon 1}\frac{\varepsilon P_{kk}}{2k} - c_{\varepsilon 2}\frac{\varepsilon^2}{k} + \frac{\partial}{\partial x_k}\left(c_\varepsilon \overline{u_k u_l}\,\frac{k}{\varepsilon}\frac{\partial \varepsilon}{\partial x_1}\right), \tag{22}$$

with coefficients $c_{\varepsilon 1} = 1.44$, $c_{\varepsilon 2} = 1.92$ and $c_\varepsilon = 0.18$. Model 3 retains this value of c_ε but adopts $c_{\varepsilon 1} = 1.0$ and $c_{\varepsilon 2} = 1.92/(1 + 0.7AA_2^{0.5})$. The stress invariants A and A_2 are defined in the Appendix.

The transport equations for the Reynolds stresses are converted to self-similar form by analogous steps to those for the mean momentum equations in § 2. Because of the multitude of additional 'source' terms arising from the transformation, a separate examination for grid dependency was made. When wall functions were used to cover the near-wall viscous sublayer, a 100×60 grid in the (x, y)-plane was sufficient, whereas when the sublayer was fully resolved, a finer 120×80 mesh was employed. This larger number of x-direction nodes was necessitated by the highly unequal spreading rates in the two directions and the desirability of avoiding excessively elongated cells in any direction.

While, strictly, the turbulent flow results again apply to a uniform Reynolds number (as for the case of laminar flow considered in § 2), here the wall friction is much less sensitive to variations in Reynolds number. Moreover, for any single laboratory test, the change in the Reynolds number over the practical length of development is small. For example, for a development of 200 diameters (which, as we note below, is far greater than attained in any experiment) an initial Reynolds number of 30 000 would have decreased by 60%; yet, the differences in the self-similar growth rates associated with this change in Reynolds number are only about 1%.

Computations are shown first for the simple isotropization model both with and without the wall-reflection terms. From Table 1, there is a great difference between the two results. In the absence of 'wall-reflection' the spreading rates in directions normal to and parallel to the wall are nearly equal, only slightly better than the eddy-viscosity results (Craft & Launder 1999). However, the addition of the 'wall-reflection' terms, (21), induces a very strong secondary motion which leads to a lateral spreading rate $dx_{1/2}/d\tilde{z}$ more than twice as large as observed in experiments with a ratio of lateral to normal growth rates of 15. The mean velocity profiles normal to the wall, are both in excellent accord with the measured profile of Abrahamsson *et al.* (1997) provided that the computed values of $y_{1/2}$ are adopted in normalizing the results (figure 7).

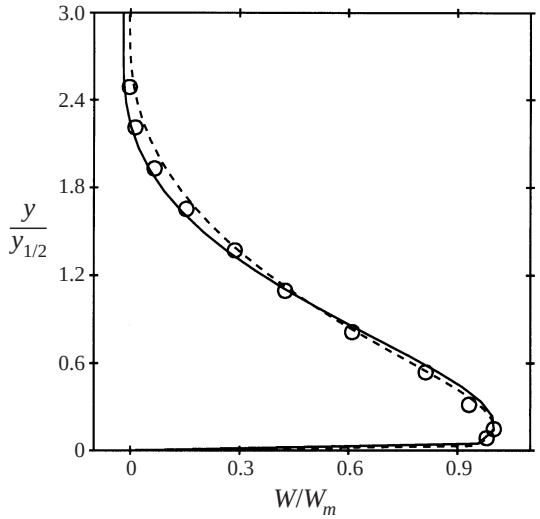

FIGURE 7. Variation of axial velocity on symmetry plane predicted by second-moment closures based on isotropization models. ——, Model 2; – – –, Model 1; Symbols: experiments of Abrahamsson *et al.* (1997).

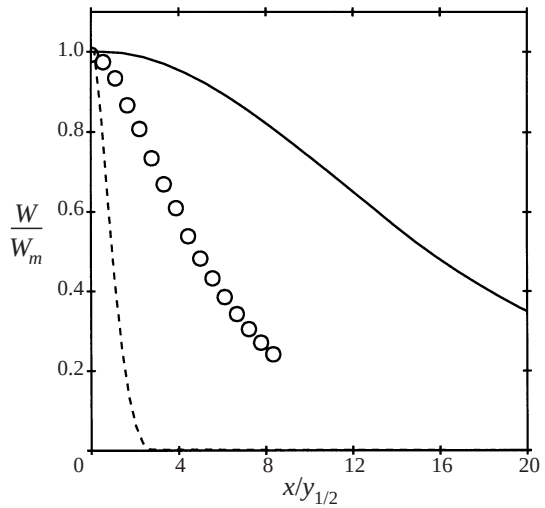

FIGURE 8. Lateral variation of axial velocity computed with isotropization models. ——, Model 2; – – –, Model 1; Symbols: experiments of Abrahamsson *et al.* (1997).

The same is equally true for the W variation with $\tilde{z}/z_{1/2}$ at a height y_m above the wall (not shown). However, if instead the lateral distance is normalized by $y_{1/2}$ (figure 8), the grave failings of both computations are strikingly brought out.

Next, attention is turned to the computed behaviour resulting from the TCL model, a scheme, it is recalled, that requires no wall-correction terms. The principal dimensionless parameters are listed in table 1 from which it is seen that the lateral rate of spread is still higher than in the experiment, though not as seriously different as with the basic model. Indeed, from figure 9, it is seen that the general shape of the axial isovels in the (x, y)-plane is very similar to those reported by Newman *et al.* (1972). The induced lateral velocity, whose profile is shown along a line parallel to the

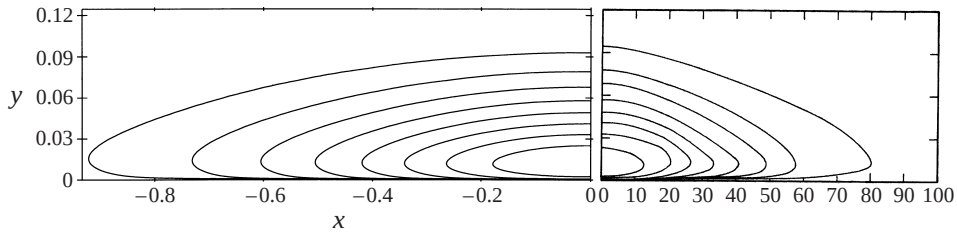

FIGURE 9. Axial velocity isovels in (x, y)-plane. Right-hand diagram: experiments, Newman *et al.* (1972). Left-hand diagram: computations with TCL model.

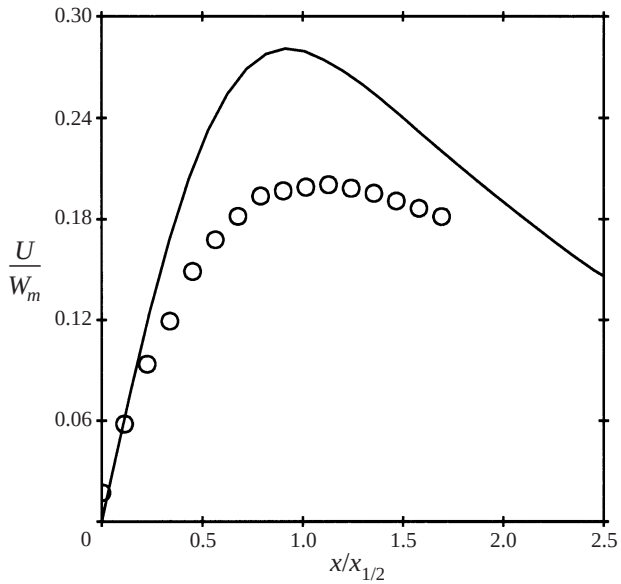

FIGURE 10. Lateral velocity along $y = y_m$. Symbols: experiments (Abrahamsson *et al.* 1997); ——, TCL computations.

wall passing through y_m in figure 10, is again of similar shape to the measured profile, though the maximum velocity is some 40% higher than Abrahamsson's reported experimental data, a figure that is consistent with the differences in the measured and computed lateral spreading rates noted above.

Extending the TCL scheme to enable integration through the viscosity-affected sublayer to the wall does not significantly alter the spreading pattern, table 1, even though the results indicate that the computed 'log-law' line lies somewhat above the level shown either in the experiments or assumed in the other computations. The general structure of the three-dimensional wall jet is, in fact, much less dependent on the wall shear stress than is, for example, the two-dimensional boundary layer. This underlines that the remaining differences between the reported experiments and the best of the computational results (Model 3) cannot be attributed to non-equilibrium viscous effects.

Finally, in this overview of the performance of different models, it is instructive to note the outcome of solving all the stress equations with the TCL model but of only applying them in the streamwise momentum equation. In the x- and y-momentum equations, an eddy-viscosity formula is used. The computations, summarized in table 2,

Source	$\frac{dy_{1/2}}{dz}$	$\frac{dx_{1/2}}{dz}$	$\frac{\dot{x}_{1/2}}{\dot{y}_{1/2}}$	$\frac{U_m}{W_m}$
Experiment (Abrahamsson *et al.* 1997)	0.065	0.32	4.94	0.2
Hybrid stress-transport/eddy-viscosity model	0.076	0.081	1.07	0.014
EVM formulation for $\overline{u^2}$, $\overline{v^2}$ only	0.064	0.137	2.14	0.093
EVM formulation for $\overline{uv}$ only	0.061	0.385	6.29	0.20

TABLE 2. Consequences of using a hybrid model (see text).

show an almost equal rate of spread in the two directions. This test thus leaves no doubt that the only significant mechanism driving the very high lateral spread of the wall jet is that of the Reynolds stress field in the (x, y)-plane in providing a source of streamwise vorticity, equation (1): the anisotropic diffusion, suggested by Davis & Winarto (1980) as the mechanism responsible, evidently plays only a very secondary role since that process will have been active in these latter computations. Proceeding further to identify the primary agent, the eddy viscosity model was next adopted just for $\overline{u^2}$ and $\overline{v^2}$ while the stress transport value for $\overline{uv}$ were retained. Then, finally, results were obtained where the stress-transport values for $\overline{u^2}$ and $\overline{v^2}$ were used while the eddy-viscosity values for $\overline{uv}$ were employed. Table 2 shows conclusively that, with the chosen axes, the normal stresses provide the principal source of streamwise vorticity.

4. Further considerations

The various explorations reported above have established that the strong lateral divergence of the three-dimensional wall jet is due, almost entirely, to the action of the Reynolds stresses in creating streamwise vorticity. As in fully developed flow in square ducts, it is the first of the Reynolds-stress terms in (1), involving the spatial variations of the differences in the normal stresses perpendicular and parallel to the wall, that is predominantly responsible for the behaviour.

Because the strength of the vorticity source is so sensitive to the computed normal stress profiles near the wall, the computed behaviour is highly dependent on the model adopted for ϕ_{ij}. The two versions tested here (Models 2 and 3) gives values of $\dot{x}_{1/2}/\dot{y}_{1/2}$ which differ by a factor of nearly 2 even though, for a two-dimensional flat-plate boundary layer, they return very similar growth rates and wall friction. Thus, the flow certainly merits inclusion as one of the standard test cases for turbulence-model assessment. (The case had in fact been selected for the 1980/81 Stanford 'Olympics' (Kline, Cantwell & Lilley 1981) but no computations were subsequently offered by participating groups.)

Nevertheless, the best of the models adopted still returned a lateral rate of spread that was 60% higher than the measurements. While not wishing to dismiss the idea that inadequacies in the turbulence model may be at least partly responsible for the remaining differences between computation and experiment, it is helpful to consider an alternative cause: that the experimental data have not, in fact, reached their self-preserving state. Certainly, it is found in other thin shear flows where there is a strong intercoupling between the axial motion and the streamwise vorticity, that it takes two or three times the development distance to reach fully developed flow as when streamwise vorticity is absent. For example, Cheah *et al.* (1993) found that for a pipe roughened with spiral flutes orientated at 30° to the pipe axis, the flow

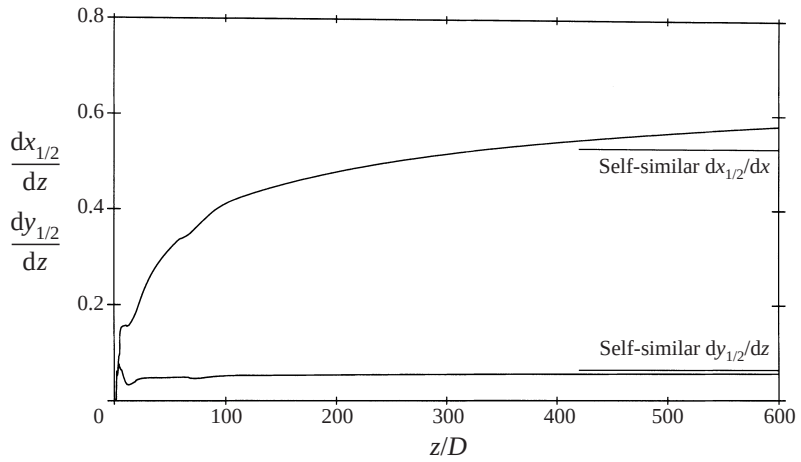

FIGURE 11. Predicted development of the wall-normal ($y_{1/2}$) and lateral ($z_{1/2}$) spreading rates.

required over 100 diameters of development to reach its fully developed state, even though roughening a pipe wall is usually held to decrease the development length. Of the relatively recent wall-jet studies, the measurements of Abrahamsson *et al.* (1997) exhibit a rapid momentum loss beyond $\tilde{z}/d = 80$ (all the comparisons made in § 3 have been with data at $\tilde{z}/d = 80$). The data of Fujisawa & Shirai (1989) which extend the furthest of any downstream seem to exhibit a steadily increasing rate of growth, though the authors represent the variation by two straight lines (the further downstream line being of greater slope).

In view of the above, we have examined the case of the developing three-dimensional wall jet in which the usual three-dimensional boundary-layer approximations have (of necessity) been made. Earlier comparison of the numerical inaccuracy arising from making this thin-shear flow approximation for the turbulent axisymmetric free jet (El Baz *et al.* 1993) showed that it led to growth rates that were too large by as much as 12% compared with that resulting from a full elliptic resolution of the Reynolds and turbulence-model equations. (It is emphasized that this difference is entirely independent of step or grid size or discretization practice; it relates purely to the equations that are solved.) We would expect errors for the three-dimensional wall jet to be similar to, but rather lower than, the above figure. Such a numerical error, while not unimportant, is small compared with the differences that arose with the fully developed results of § 3.

Attention has been limited to the TCL model since this was clearly the most successful of the schemes employed. Figure 11 shows the computed slow development of the lateral growth rate in which perceptible changes in the growth rate are still noticeable 700 initial jet diameters downstream. In figure 12 we show the developing velocity profiles for the axial and lateral motion, respectively. From this, it is evident that at roughly 100 jet diameters downstream, the lateral variation of the axial and lateral velocity profiles is in reasonable accord with experiments. (Obi (1997) has also contributed developing flow computations for the three-dimensional wall jet. His model, a variant of the basic model, returned lateral spreading rates nearly twice as high as the TCL model but confirmed that full development had not been reached by $z/D = 180$.)

Concerning the r.m.s. velocity profiles, it is noted first that in figure 13 on the

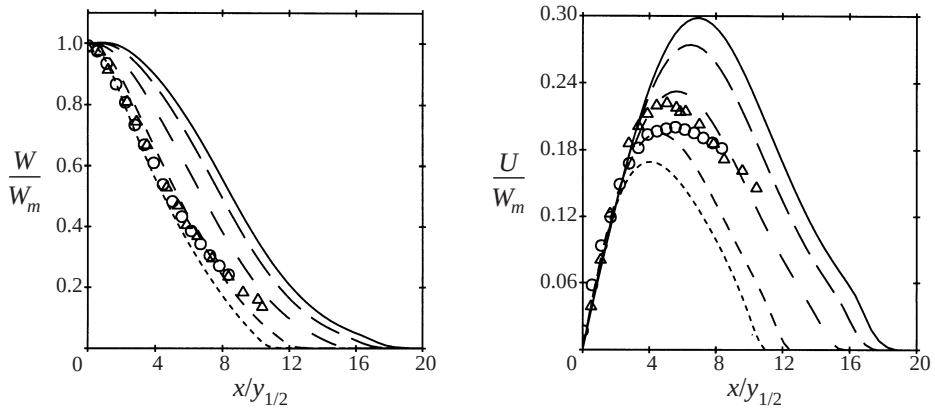

FIGURE 12. Profiles of the streamwise and lateral velocity along $y = y_m$ at a selection of downstream distances. - - -, $z/D = 50$; – – –, 100; — —, 200; — —, 400; —— ——, 600. ○, Experiments of Abrahamsson *et al.* (1997); △, Experiments of Fujisawa & Shirai (1986).

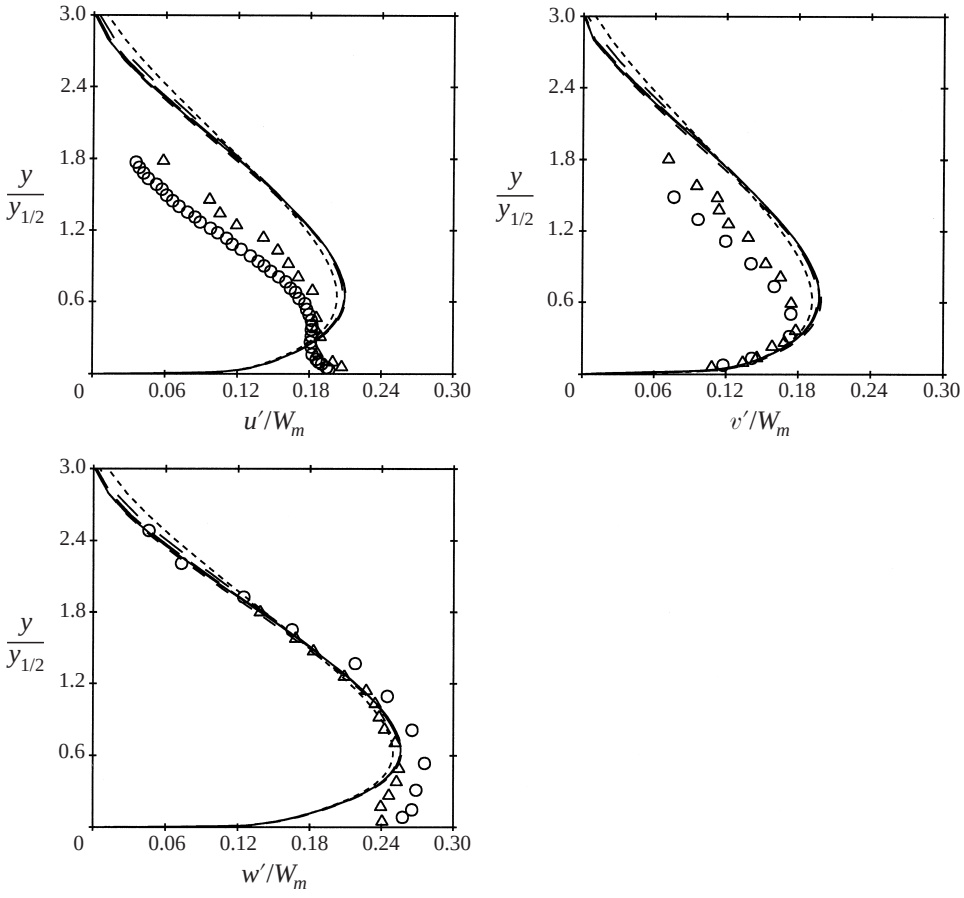

FIGURE 13. Profiles of r.m.s. velocities on the symmetry plane at a selection of downstream distances. Key as figure 11.

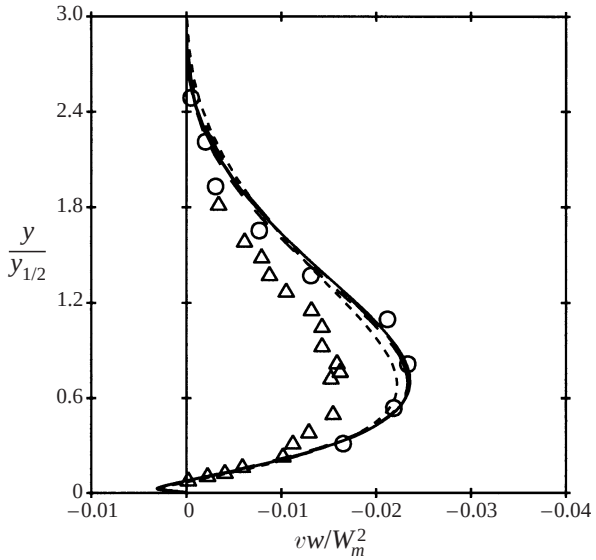

FIGURE 14. Profiles of turbulent shear stress on the symmetry plane. Key as figure 11.

symmetry plane there is scarcely any difference between computed profiles at different streamwise stations. This perhaps helps to explain why those presenting experimental results have felt justified in asserting their flow to have reached the fully developed limit. Agreement with experiment is fairly good for w' (streamwise) v' (normal), but is substantially different for u' (lateral). This may possibly indicate an inadequate accounting of the 'splat' effect in the model. The shear stress, figure 14, accords closely with Abrahamsson's experiments.

There is, figure 15, a greater lateral variation in the r.m.s. profiles, with downstream distance. Along the line considered ($y = y_m$, the position of maximum velocity at $x = 0$), the measured u' and w' levels are rather higher than the computations, though the shape is similar. The v' profile at $z = 100D$ is in close agreement with the experimental data.

5. Conclusions

This computational exploration of the three-dimensional turbulent wall jet has settled many of the physical issues concerning the flow: specifically, that the high lateral rate of spread is due entirely to induced axial vorticity rather than to asymmetric diffusion and that the driving vorticity source is created by the anisotropy of the Reynolds stresses in the plane perpendicular to the jet axis rather than to the bending of mean vortex lines. Thus, the source is precisely the same as that driving secondary motions in straight non-circular ducts. There is an important difference, however: in ducts these motions are of the order of 1% of the primary motion while in the wall jet they are fully an order of magnitude greater.

The main computational effort has been directed at second-moment closure. At this level, it has been demonstrated that the predicted flow pattern is extremely sensitive to the particular pressure-strain model (ϕ_{ij}) adopted. The two-component-limit model, developed for free flows a decade ago and subsequently applied to flow in straight and curved square ducts, is clearly more successful than the simpler variants tested.

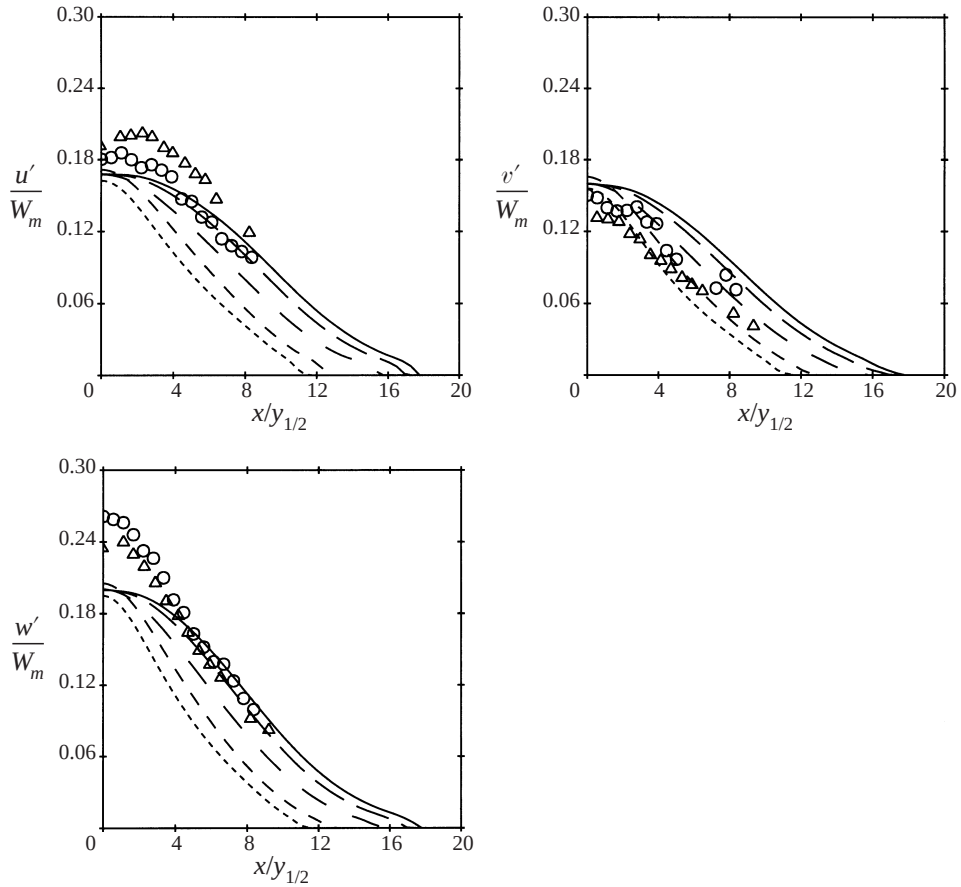

FIGURE 15. Profiles of r.m.s. velocities along $y = y_m$. Key as figure 11.

Precisely how successful it is, cannot currently be ascertained directly because evidence from developing flow computations indicates that the flow has by no means reached full development by 100 initial diameters of flow development. The slow evolution rate arises from the intercoupling of the secondary flow and the primary motion and the fact that the secondary flows are strong enough to modify the Reynolds stresses which are, in turn, the drivers of the secondary currents.

Finally, it may be observed that, since the three-dimensional wall jet is an acutely sensitive flow for assessing turbulence models, it would be desirable to establish definitive experimental or, possibly, LES results for the fully developed limit (so that uncertainties about the precise state of the flow at the inlet have no bearing on the flow character). In view of the difficulties associated with carrying out accurate experiments that extend several hundred diameters downstream, it is likely that performing an LES computation, using the fully devleoped-flow strategy adopted for duct flow computations, would provide the best way of establishing this basic data.

T. J. C. expresses his appreciation to The Royal Society of London for support through a University Research Fellowship. Mrs C. King has prepared the paper for publication. Authors' names appear alphabetically.

Appendix

In Model 3 the pressure correlation terms are modelled as

$$\phi_{ij} = \phi_{ij1} + \phi_{ij2} \tag{A 1}$$

and the forms for ϕ_{ij1} and ϕ_{ij2} can be written as

$$\begin{aligned}
\phi_{ij1} &= -c_1\varepsilon[a_{ij} + c_1'(a_{ik}a_{kj} - \tfrac{1}{3}A_2\delta_{ij})] - \varepsilon a_{ij} \\
\phi_{ij2} &= -0.6(P_{ij} - \tfrac{1}{3}\delta_{ij}P_{kk}) + 0.3a_{ij}P_{kk} \\
&\quad -0.2\left[\frac{\overline{u_ku_j}\;\overline{u_lu_i}}{k}\left[\frac{\partial U_k}{\partial x_l} + \frac{\partial U_l}{\partial x_k}\right] - \frac{\overline{u_lu_k}}{k}\left[\overline{u_iu_k}\,\frac{\partial U_j}{\partial x_l} + \overline{u_ju_k}\,\frac{\partial U_i}{\partial x_l}\right]\right] \\
&\quad -c_2[A_2(P_{ij} - D_{ij}) + 3a_{mi}\,a_{nj}(P_{mn} - D_{mn})] \\
&\quad +c_2'\left\{\left(\frac{7}{15} - \frac{A_2}{4}\right)(P_{ij} - \tfrac{1}{3}\delta_{ij}P_{kk})\right. \\
&\qquad +0.1[a_{ij} - \tfrac{1}{2}(a_{ik}a_{kj} - \tfrac{1}{3}\delta_{ij}A_2)]P_{kk} - 0.05a_{ij}a_{lk}P_{kl} \\
&\qquad +0.1\left[\left(\frac{\overline{u_iu_m}}{k}P_{mj} + \frac{\overline{u_ju_m}}{k}P_{mi}\right) - \frac{2}{3}\delta_{ij}\frac{\overline{u_lu_m}}{k}P_{ml}\right] \\
&\qquad +0.2\,\frac{\overline{u_lu_i}\;\overline{u_ku_j}}{k^2}(D_{lk} - P_{lk}) \\
&\qquad +0.1\left[\frac{\overline{u_lu_i}\;\overline{u_ku_j}}{k^2} - \frac{1}{3}\delta_{ij}\,\frac{\overline{u_lu_m}\;\overline{u_ku_m}}{k^2}\right] \\
&\qquad \left.\times\left[6D_{lk} + 13k\left[\frac{\partial U_l}{\partial x_k} + \frac{\partial U_k}{\partial x_l}\right]\right]\right\},
\end{aligned} \tag{A 2}$$

where $D_{ij} = (\overline{u_iu_k}\,\partial U_k/\partial x_j + \overline{u_ju_k}\,\partial U_k/\partial x_i)$,

$$a_{ij} = \overline{u_iu_j}/k - \tfrac{2}{3}\delta_{ij}, \quad A_2 = a_{ij}a_{ij}, \quad A_3 = a_{ij}a_{jk}a_{ki}, \quad A = 1 - \tfrac{9}{8}(A_2 - A_3)$$

$$c_1 = 3.1(AA_2)^{0.5}, \quad c_1' = 1.1,$$

$$c_2 = \min(0.55(1 - \exp(-A^{1.5}R_t/100)), 3.2A/(1 + S)),$$

$$c_2' = \min(0.6, A) + 3.5(S - \Omega)/(3 + S + \Omega) - 2.0S_I,$$

$$S = \frac{k}{\varepsilon}\sqrt{S_{ij}S_{ij}/2}, \quad \Omega = \frac{k}{\varepsilon}\sqrt{\Omega_{ij}\Omega_{ij}/2}, \quad S_I = S_{ij}S_{jk}S_{ki}/(S_{st}S_{st}/2)^{1.5}.$$

The dissipation ε_{ij} and diffusion d_{ij} are approximated using local isotropy and the generalized gradient diffusion hypothesis, respectively, and are thus again modelled via equations (18) and (19).

REFERENCES

Abrahamsson, H., Johansson, B. & Löfdahl, L. 1997 An investigation of the turbulence field in the fully developed three-dimensional wall-jet. *Internal Rep* 97/1, Chalmers University of Technology, Sweden.

Black, A. W. & Sparrow, E. M. 1970 *Trans. ASME C: J. Heat Transfer* **89**, 258–268.

Brundrett, E. & Baines, W. D. 1964 *J. Fluid Mech.* **19**, 375.

Carr, A. D., Connor, M. A. & Buhr, H. O. 1973 *Trans. ASME C: J. Heat Transfer* **95**, 445–452.

Cheah, S. C., Cheng, L., Cooper, D. & Launder, B. E. 1993 *Proc. 5th IAHR Conf. on Refined Flow Modelling and Turbulence Measurement*, pp. 269–276. Presses Ponts et Chaussées, Paris.

Chieng, C. C. & Launder, B. E. 1979 *Numer. Heat Transfer* **2**, 359–371.

Craft, T. J. 1997 Computations of separating and re-attaching flow using a low-Reynolds-number second-moment closure. Paper 30–19, Proc. 11th Symp. Turbulent Shear Flows, Grenoble.

Craft, T. J. & Launder, B. E. 1992 *AIAA J* **30**, 2970–2972.

Craft, T. J. & Launder, B. E. 1999 The self-similar, turbulent, three-dimensional wall jet. *Proc. 1st Symp. on Turbulent Shear Flow Phenomena*, Santa Barbara.

Craft, T. J., Launder, B. E. & Ince, N. Z. 1996 *Dyn. Atmos. Oceans*, **23**, 99–114.

Daly, B. J. & Harlow, F. H. 1970 *Phys. Fluids* **13**, 2634–2649.

Davis, M. R. & Winarto, H. 1980 *J. Fluid Mech.* **101**, 201–221.

Durbin, P. 1993 *J Fluid Mech.* **249**, 465–498.

El Baz, A., Craft, T. J., Ince, N. Z. & Launder, B. E. 1993 *Intl J. Heat Fluid Flow* **14**, 164–169.

Fu, S. 1988 Computational modelling of turbulent swirling flows with second-moment closures. PhD Thesis, Faculty of Technology, University of Manchester.

Fu, S., Launder, B. E. & Tselipidakis, D. 1987 Accommodating the effects of high strain rates in modeling the pressure–strain correlation. Rep. TFD/87/5, Mech. Engng Dept, UMIST.

Fujisawa, N. & Shirai, H. 1989 *Trans. Japan Soc. Aerospace Sci.* **32**, 35–46.

Glauert, M. B. 1956 *J. Fluid Mech.* **1**, 625–643.

Hanjalic, K. & Obi, S. (ed.) 1997 *Proc. 6th ERCOFTAC/IAHR/COST Workshop on Refined Flow Modelling*. Delft University of Technology.

Iacovides, H., Launder, B. E. & Li, H.-Y. 1996 *Expt Thermal Fluid Sci.* **13**, 419–429.

Jones, W. P. & Launder, B. E. 1972 *J. Fluid Mech.* **56**, 337–351.

Kebede, W. 1982 Numerical study of the self-preserving three-dimensional wall-jet. MSc dissertation, Faculty of Technology, University of Manchester.

Kline, S. J., Cantwell, B. J. & Lilley, G. M. (ed.) 1981 *Proc. 1980–81, AFOSR-HTTM, Stanford Conf. on Complex Turbulent Flow*, vol. 1, p. 439. Stanford.

Kudva, A. K. & Sesonke, A. 1972 *Intl J. Heat Mass Transfer* **15**, 127.

Launder, B. E. & Li, S.-P. 1994 *Phys. Fluids* **6**, 999–1016.

Launder, B. E. & Rodi, W. 1981 *Prog. Aerospace Sci.* **19**, 81–128.

Launder, B. E. & Rodi, W. 1983 *Ann. Rev. Fluid Mech.* **15**, 429–459.

Launder, B. E. & Sharma, B. I. 1974 *Lett. Heat Mass Transfer* **1**, 131–138.

Lien, F.-S. & Leschziner, M. A. 1993 *Turbulent Shear Flows*, vol. 8, pp. 205–222 (ed. F. Durst *et al.*). Springer.

Lumley, J.-L. 1978 *Adv. Appl. Mech.* **18**, 123.

McGuirk, J. J. & Rodi, W. 1978 Mathematical modelling of three-dimensional heated surface jets. SFB 80, Rep. T/135, University of Karlsruhe.

Matsuda, H., Iida, S. & Hayakawa, M. 1990 *Trans. ASME I: J. Fluids Engng* **112**, 462–467.

Newman, B. G., Patel, R. P., Savage, S. B. & Tjio, H. K. 1972 *Aero Q.* **23**, 693–698.

Obi, S. 1997 Description of numerical aspects and turbulence models: the three-dimensional wall-jet. In *Proc. 6th ERCOFTAC/IAHR/COST Workshop.*

Padmanabham, G. & Gowda, B. H. L. 1991 *J. Fluids Engng* **113**, pp. 620–628, 629–634.

Patankar, S. V. & Spalding, D. B. 1972 *Intl J. Heat Mass Transfer* **15**, 1787.

Rhie, C. M. & Chow, W. L. 1983 *AIAA J.* **21**, 1525.

Schlichting, H. 1933 *Z. angew Math. Mech.* **13**, 260.

Shih, T.-H. & Lumley, J.-L. 1985 Modeling of pressure correlations in Reynolds stress and scalar flux equations. Rep. FDA-85-3, Sibley School of Mech. Aerospace Engng Cornell University.

Van Leer, B. 1979 *J. Comput. Phys.* **32**, 101.

Wizman, V., Laurence, D., Kanniche, M., Durbin, P. & Demuren, O. 1996 *Intl J. Heat Fluid Flow*, **17**, 255–266.